CHEMISTRY OF MATERIALS

Article

pubs.acs.org/cm

Hierarchically Designed Germanium Microcubes with High Initial Coulombic Efficiency toward Highly Reversible Lithium Storage

Chuanjian Zhang,[†] Zhou Lin,[†] Zhenzhong Yang,[‡] Dongdong Xiao,[‡] Pu Hu,[†] Hongxia Xu,[†] Yulong Duan,[†] Shuping Pang,[†] Lin Gu,*[,‡] and Guanglei Cui*[,†]

[†]Qingdao Industrial Energy Storage Research Institute, Qingdao Institute of Bioenergy and Bioprocess Technology, Chinese Academy of Sciences, No. 189 Songling Road, Laoshan District, Qingdao, 266101, P. R. China

[‡]Beijing Laboratory for Electron Microscopy, Institute of Physics, Chinese Academy of Sciences, No. 8, 3rd South Street, Zhongguancun, Haidian District, Beijing 100190, P. R. China

Supporting Information

ABSTRACT: Germanium has been investigated intensively for its high specific capacity and tough nature, which make it a promising candidate anode for high energy lithium-ion batteries. However, the rational design of a germanium electrode with enhanced electrochemical performances is still a big challenge. Herein, we designed and synthesized germanium microcubes with a hierarchical structure directly on titanium foil via a simple hydrogen reduction method. An ultrahigh initial Coulombic efficiency of 91.8% was acquired due to the high crystallinity of germanium for reversible lithium insertion and extraction, less adverse side reaction for irreversible lithium loss, and unique hierarchical structure for easier electrolyte penetration. In addition, the Li_2CO_3-predominated solid electrolyte interface contributes significantly to the excellent cycling and rate performances of the anode. Both half and full cell performances demonstrate that germanium has potential applications in high-performance lithium-ion batteries.

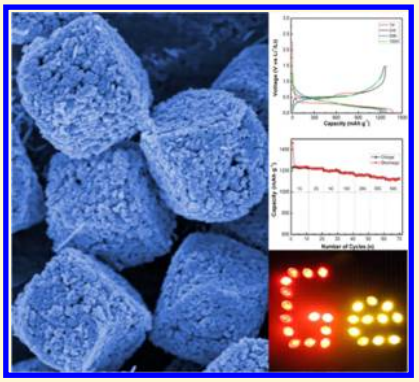

INTRODUCTION

Group IV semiconductors known for their significantly high capacities have aroused great interests as the most promising anodes for high power lithium-ion batteries (LIBs).[1,2] Compared with Si, Ge possesses a superior lithium diffusivity and electrical conductivity, which implies an excellent rate capability.[3,4] Additionally, a better oxidation resistance than Si makes Ge an ideal model to investigate the Li storage behavior in alloy anodes.[5,6] Although the higher cost limits its commercial application to some extent, the Ge anode has successfully gained enough attention for its mentioned merits.[7−9] Unfortunately, Ge also undergoes a huge volume expansion (370%) during lithiation, which leads to electrode pulverization. Therefore, severe capacity fade is generally observed for Ge-based anodes, and considerable efforts have been directed at addressing the problem. Because the alloying/dealloying kinetics of the electrodes are highly dependent on their morphologies and microstructures, nanosized Ge materials such as nanowires,[10−12] nanotubes,[13,14] and nanorods[15] exhibited enhanced cycle stability due to their one-dimensional structural feature. It is true that downsizing the particle size to nanoscale could increase the rate of ion and electron migration;[16,17] however, the resistance increase between isolated nanocomponents and the high reactivity of nanoparticles also cannot be ignored, both of which are detrimental to their cycling performances. As reported, it might be a better way to address this issue by constructing active particles on the microscale which are composed of the hierarchical nanostructures.[18,19]

Moreover, the alloy anodes also suffer from another challenge of low Coulombic efficiency, which is very detrimental for their commercial application.[3,7,16] Because of the remarkable volume change of the crystal lattice during lithium insertion and extraction, Si and Ge pulverize, accompanying the formation and repair of solid electrolyte interphase (SEI).[20] In this case, a large amount of lithium will be consumed and low Coulombic efficiency, especially low initial Coulombic efficiency, is (below 80%) always observed.[7,13,21] According to Wachtler et al.'s research,[22] the reasons for the low Coulombic efficiency in the first charge/discharge cycle of an alloy anode lie in four aspects: formation of SEI caused by electrolyte decomposition, adverse side reactions between inactive components and lithium metal, electrical contact failure of electrode, and irreversible trapping of lithium in host metals. On the other hand, the favorable SEI layer may be very essential to the cycling stability of the anode. In addition, the strategies that construct active materials directly on the current collector without binder and conductive carbon were reported to be helpful for the improvements of battery performances.[23,24] Therefore, if we could hierarchically design and construct a monolithic anode with high crystallinity for

Received: January 18, 2015
Revised: February 18, 2015
Published: February 26, 2015

DOI: 10.1021/acs.chemmater.5b00218
Chem. Mater. 2015, 27, 2189−2194

favorable lithium insertion/deinsertion, a high initial Coulombic efficiency and enhanced cycling performance could be expected.

With the aim of improving Coulombic efficiency especially for the first cycle, we developed monolithic Ge microcubes which are composed of nano-building blocks as anode for LIBs. Material characterizations confirm that the Ge microcubes have a good crystallinity with few surface oxide contamination, which was responsible for the ultrahigh initial Coulombic efficiency of 91.8%. Due to the asymmetric rate feature, the monolithic anodes exhibit a remarkable delithiated capacity of 1121 mAh g^{-1} at 50 C. Full cell performances based on Ge microcubes were also explored.

EXPERIMENTAL SECTION

Preparation of Germanium Microcubes. Initially, 0.5 g of GeO_2 raw powders (Aladdin reagent) was dissolved in 30 mL of 3 wt % ammonia solution, followed by stirring at 70 °C for 30 min, and a transparent germanate ion solution was obtained. A dilute phosphoric acid was added to adjust the pH value of the solution to ~2. Titanium foil with a thickness of 100 μm (GoodFellow) was punched into a disk with a diameter of 10 mm and employed as substrate, which has been put into germinate ion solution for 12 h liquid phase deposition reaction. After it was dried in an electrical oven at 60 °C for 12 h, a Ti substrate with white GeO_2 microcubes film was obtained. For synthesis of Ge microcubes, Ti foil with the as-deposited GeO_2 was thermally treated at 550 °C for 1 h under a hydrogen atmosphere with a pressure of 0.25 bar.

Materials Characterization. X-ray diffraction (XRD) patterns of samples were recorded on a Bruker-AXS Micro-diffractometer (D8 ADVANCE) with Cu Kα radiation (λ = 1.5406 Å) from 10° to 90° at a scanning speed of 4° min^{-1}. Morphology details and lattice structural information were examined using field emission scanning electron microscopy (FESEM, HITACHI S-4800) and high-resolution transmission electron microscopy (HRTEM, TECNAI F20 ST). The Fourier transform infrared spectroscopy (FTIR) data were acquired on a Bruker TENSOR 27 spectrometer inside an Ar-purged chamber. X-ray photoelectron spectroscopy (XPS) was acquired using an ESCALab220i-XL spectrometer (VG Scientific) with Al Kα radiation in twin anodes at 14 kV × 16 mA. Both FTIR and XPS tests were conducted on the same anodes extracted from cycled coin cells after rinsing with DMC and drying overnight in a vacuum. The *in situ* TEM measurement was employed to detect the morphology evolution during the first lithiation and was carried out using a nanobattery configuration with Ge nanoparticles as anode, Li metal as cathode, and Li_2O as solid electrolyte, as reported previously.[25,26]

Electrochemical Analysis. Electrochemical measurements were performed using CR2032 coin-type cells assembled in an argon-filled glovebox. The half cells were assembled using the Ge microcubes monolithic cathode, a Li metal foil as the anode, a polypropylene separator (Celgard 2500), and a liquid electrolyte (ethylene carbonate, dimethyl carbonate, and dimethyl carbonate, 1:1:1 by volume) with 1.0 M $LiPF_6$ and 5 wt % vinylene carbonate (VC) additive. Full cells were fabricated by using a $LiFePO_4$ cathode and a Ge microcubes anode. The assembled half cells were cycled between 0.005 and 1.5 V, while the full cells were charged and discharged between 2.3 and 3.3 V using a LAND battery testing system. Electrochemical impedance spectroscopy (EIS) measurements of the Ge microcubes with different lithiated states were carried out using a ZHANER ZENNIUM electrochemical workstation by applying an AC voltage of 5 mV amplitude in the frequency range of 0.1−100 kHz at room temperature.

RESULTS AND DISCUSSION

A schematic illustration of the fabrication process for the Ge microcubes is depicted in Figure 1. GeO_2 microcubes were first synthesized via a simple liquid phase deposition (LPD) process

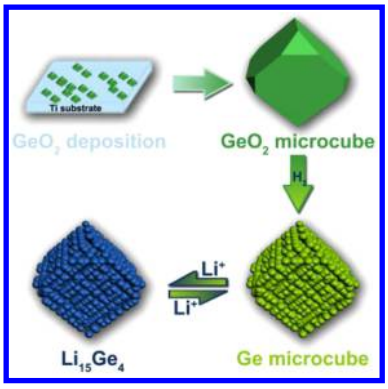

Figure 1. Schematic diagram for the fabrication of a porous Ge microcube on titanium foil.

and deposited directly onto a titanium foil. Sharp XRD peaks in Figure S1 (Supporting Information), which were well indexed to the hexagonal phase (JCPDS No. 36-1463), indicated only a hexagonal GeO_2 crystal existed on the Ti electrode. SEM images in Figure S2 (Supporting Information) reveal that the LPD-derived GeO_2 sample shows a truncated cube morphology and a solid surface with a particle size of around 3 μm. The second and the most essential step is to reduce the oxide precursor to metallic Ge. During the reduction process, GeO_2 cubes are etched by hydrogen, which leads to a transformation from a solid to a micro/nano architecture.

As shown in Figure 2a, the oxide cube has completely transformed into diamond cubic Ge (JCPDS No. 04-0545)

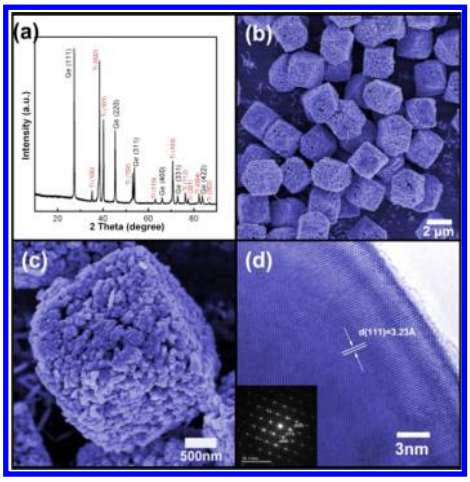

Figure 2. Typical XRD pattern (a), SEM images (b, c), and high-resolution TEM image of Ge microcubes (d). Inset in (d) is the corresponding selected area electron diffraction (SAED).

after being annealed in a hydrogen atmosphere.[27,28] The narrow peak width indicates that the as-synthesized Ge microcubes have a good crystalline quality. Detailed morphology information on the cubes was investigated by scanning electron microscopy (SEM) and high-resolution transmission electron microscopy (HRTEM). It is interesting to observe from Figure 2b,c that all the Ge microcubes are composed of numerous primary particles with sizes of tens of nanometers, which may be helpful for electrolyte penetration and ion diffusion.[29] Such hierarchical structures are commonly observed in metal oxides from thermal decomposition of the corresponding carbonates reported by Lou's group, but seldom

DOI: 10.1021/acs.chemmater.5b00218
Chem. Mater. 2015, 27, 2189−2194

found in Ge and Si structures.[30−32] In our case, the porous Ge microcubes are shaped by the removal of oxygen from the solid oxide cubes. A HRTEM image taken on the edge of an individual Ge nanoparticle in Figure 2d shows clear lattice fringes, which indicates a highly ordered crystalline structure of Ge particle with a (111) interplanar spacing of 3.22 Å. Only a minimal detectable oxide layer is observed in HRTEM image because of the better oxidation resistance of Ge, which also could be confirmed by the XPS results (Figure S3, Supporting Information). The selected area electron diffraction (SAED) pattern in the inset of Figure 2d, taken along the [011] zone axis from an individual nanoparticle, shows sharp diffraction spots, indicating again that the as-synthesized Ge microcubes have a good crystallinity. It is reported that Ge powders with an amorphous structure may hinder the reversible lithiation process, which leads to a low Coulombic efficiency.[21] In our case, highly ordered Ge atoms arrangement and less surface contamination may decrease the amount of trapped Li in the host material, as well as the Li consumption due to the reduction of the oxide layer.[33] Afterward, Ti foils with Ge microcubes were evaluated as monolithic anodes free of inactive materials (for example, binder and carbon black) for LIBs with the mass loading of about 2 mg cm^{-2}. As a consequence, an improved initial Coulombic efficiency could be expected.

Representative charge/discharge profiles of Ge microcubes at 0.1 C (1 C = 1384 mA g^{-1} according to $Li_{15}Ge_4$) are plotted in Figure 3a. The discharge curve for the first cycle exhibits a very

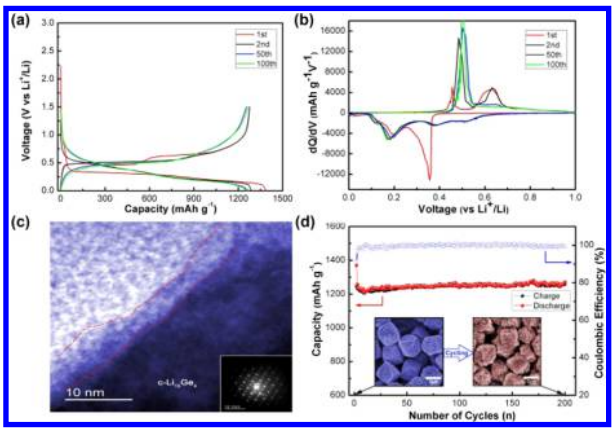

Figure 3. (a) Voltage profiles and (b) the corresponding differential capacity plot of the 1st, 2nd, 50th, and 100th cycle of the Ge microcubes in the voltage range of 0.005−1.5 V vs Li^+/Li at 0.1 C (1 C = 1384 mA g^{-1} according to $Li_{15}Ge_4$). (c) HRTEM image of the fully lithiated $Li_{15}Ge_4$ (5 mV), in which the SEI layer is marked by red lines. (d) Cycling performance of Ge microcubes and Coulombic efficiency at a rate of 0.1 C. Inset in (d) is the SEM image of Ge microcubes before the cycle and after 200 cycles, respectively.

flat plateau around 0.3 V due to the formation of a Li−Ge alloy. For the first charge process, it offers two delithiation platforms below 0.7 V, which is very similar to that of Ge/C nanostructures reported by the previous literature.[4] In order to clarify the lithium storage mechanism of Ge microcubes, *ex situ* XRD measurements were performed, and the patterns are shown in Figure S4 (Supporting Information). Interestingly, the fully discharged product is ascribed to $Li_{15}Ge_4$ rather than $Li_{22}Ge_5$, which corresponds to a theoretical capacity of 1384 mAh g^{-1}.[34] The discharge and charge capacities of the Ge microcubes for the first cycle were 1388 and 1275 mAh g^{-1} at the rate of 0.1 C, respectively, which corresponded to an initial Coulombic efficiency of 91.8%, which is comparable with the best result (91%) reported by Cho's group.[35] It is worth noting that the hierarchical architecture is favorable for liquid electrolyte penetration and all the active Ge nanoparticles could participate into the electrochemical reactions to realize a maximum storage of lithium. At the same time, high crystallinity of the as-synthesized Ge guarantees that the lithium will extract from the host reversibly. In addition, the absence of inactive materials in the electrode, free of surface oxide layer contamination, combined with the micro/nano structure were considered as the main reasons for the high initial Coulombic efficiency of 91.8%. Both the charge and discharge curves of the second cycle are in good accordance with those of the subsequent cycles, which demonstrate a highly reversible lithium insertion and exaction behavior.

The corresponding differential capacity profiles are plotted in Figure 3b. During the first cycle, a sharp peak centered at 0.36 V, which is accompanied by two broad peaks located at 0.1−0.2 V, was detected. The former is related to the lithiation induced amorphization of crystalline Ge, and the latter corresponds to the further lithium insertion of amorphous Ge, which results in the formation of amorphous Li_xGe.[5,12,13] There are no detectable peaks associated with SEI formation, and the reduction of the oxide layer appeared at the voltage range between 0.5 and 1 V, which indicated a less irreversible lithium consumption on account of the side reaction.[8] Afterward, for the first charge process, the fully discharged product $Li_{15}Ge_4$ experiences a stepwise removal of lithium, which accounts for the two delithiation peaks with weak intensity at 0.45 and 0.63 V.[8,12] In the subsequent cycles, the sharp Li-insertion peak at 0.36 V was replaced by a series of broad peaks with low intensity due to the lithiation of amorphous-Ge. According to the Korgel group's research, one of the clearest signatures of capacity fade was the disappearance of the sharp delithiation peak at 0.5 V.[12] For our case, the prominent lithium extraction peak at 0.51 V still exists with high intensity even after the 100 cycles, which implies that the as-synthesized Ge anode may exhibit high capacity retention. *In situ* TEM images (Figure S5, Supporting Information) clearly show the morphology evolution for the lithium insertion process. During lithiation, crystalline Ge nanoparticles became amorphous gradually to form a-Li_xGe and finally transformed to c-$Li_{15}Ge_4$ alloy, which accompanies a volume expansion rate of about 230%. In this stage, cracks were not observed, which implied a good lithium accommodation behavior. This is because of the weak anisotropy of the lithiation strain at the reaction front which makes Ge nanoparticles tough for lithium insertion, as reported by Zhang and his colleagues.[26] The clear lattice fringe and sharp spots in the HRTEM image (Figure 3c) confirm that $Li_{15}Ge_4$ possesses a good crystallinity. A thin SEI layer was also observed on the surface of the fully discharged Ge anode. It was reported that the SEI was predominately composed of inorganic Li_2CO_3 and LiF when the electrode was fully discharged.[36] The tough nature of the Ge crystal and stable SEI indicate that the Ge microcube has the potential to realize good capacity retention. As is expected, the anode delivers a reversible capacity of 1250 mAh g^{-1} up to 200 cycles with a capacity retention of 99% at 0.1 C in Figure 3d. More importantly, *ex situ* SEM images in the inset confirmed that the Ge microcube maintained good morphology integrity without structure failure after 200 cycles.

DOI: 10.1021/acs.chemmater.5b00218
Chem. Mater. 2015, 27, 2189−2194

Nowadays, studies have shown that a Ge-based anode could maintain high and stable capacities at high charge rates if the materials discharged at a fixed and slower rate.[8,12] Therefore, the electrodes both cycled at a fixed and progressive discharge rate were performed (Figure 4a and Figure S6, Supporting Information). Obviously, the Ge microcubes show much more stable rate capability and minimal capacity fade when lithiate at a rate of 1 C. Specifically, at charge rates of 10, 20, and 30 C, the Ge anode exhibited capacities of 1118, 1155, and 1131 mAh g^{-1}, respectively. Even if the electrode was cycled at a very high rate of 50 C, a charge capacity of 1121 mAh g^{-1} was acquired, which was 90% of the initial charge capacity (1234 mAh g^{-1}) at 1 C. More recently, Dudney, Xiao, and co-workers[37] reported a similar asymmetric rate behavior for a Si anode, which means a high capacity retention was achieved at a low lithium insertion rate but an ultrahigh extraction rate. They ascribed this phenomenon to the potential-concentration profile and voltage shift caused by Ohmic resistance under high current, which may also explain the ultrahigh charge capacity for our Ge anode. Moreover, long cycling stability of the Ge anode at 1 C was also evaluated and is shown in Figure 4b. After 500 charge/discharge cycles, the electrode displayed a reversible capacity of 1204 mAh g^{-1}, corresponding to a 94.1% capacity retention from the first cycle (1279 mAh g^{-1}), indicative of a good cycling stability.

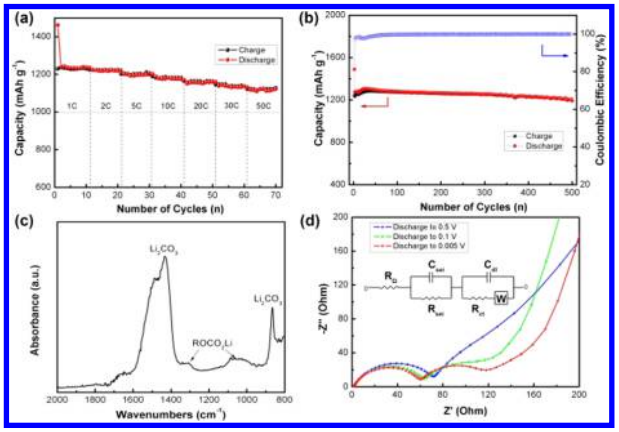

Figure 4. (a) The capacities of the Ge electrode charged and discharged at varied current densities. The charge rates were varied from 1 to 50 C for every 10 cycles, while the discharge rate was kept constant at 1 C for all cycles. (b) Cycling performance of Ge microcubes and Coulombic efficiency at a rate of 1 C. (c) FTIR spectrum of fully lithiated Ge electrode surface (0.005 V). (d) Nyquist plots and the corresponding equivalent circuit of the Li/Ge half cell at different lithiated voltages for the first cycle. The current density for discharge is 1 C.

We consider this excellent rate capability should be related to the stable SEI layer. As shown in Figure 4c, the strong FTIR bands at 1439 and 866 cm^{-1} are the direct evidence that the predominant species in SEI is Li_2CO_3 rather than lithium alkylcarbonates ($ROCO_2Li$).[38−40] XPS spectra (Figure S7, Supporting Information) further confirmed this result. It is known that stable SEI on the surface of an anode, especially generated during the first lithiation process, is essential to suppress the capacity decay.[41] In our case, the micro/nano architecture allows the liquid electrolyte to penetrate easily into the active materials and decompose to form the SEI layer during the first lithiation homogeneously. Furthermore, the monolithic electrode fabricated without conductive additive and binder may also suppress the side reactions. Additionally, the stronger FTIR and XPS peaks compared with the previous literatures demonstrate that it is the Li_2CO_3-predominated SEI layers which lead to the Ge microcubes possessing an excellent cycling performance.[25]

Afterward, in order to clarify how the lithiation rate may affect their performances, electrochemical impedance spectroscopy (EIS) of Ge microcubes at different discharged states was employed. All the Nyquist plots of Ge microcubes at various voltages (Figure 4d) are composed of two compressed semicircles and a straight line. The corresponding equivalent circuit is displayed in the inset. At a lower discharge rate (1 C), as more lithium inserts into the Ge host lattice, R_{SEI} and R_{ct} exhibit more compressed with the voltage decline, which implies a more favorable SEI formation for lithium diffusion. This may be due to the deposition of highly lithium conductive Li_2CO_3 on the surface of the electrode below 0.5 V.[36,42] However, when increasing the lithium insertion current to 10 C (Figure S8, Supporting Information), the impedance pattern changes considerably. The second semicircle becomes much more suppressed, and the inclined line in the low-frequency range almost disappears. The lack of the straight line with a reasonable slope is indicative of suppressed insertion of lithium in the bulk of the material due to the absence of well-formed SEI.[42] The stable SEI layer, which is beneficial to the cycling stability, may be only formed under moderate intercalation current. Additionally, it is reported that the formed Li_xGe alloy exhibits metallic properties, which enhances its conductivity.[43] A slower lithiation condition is believed to be more favorable for the formation of conductive $Li_{15}Ge_4$ and finally improves the rate capability when discharged at a fixed and lower rate.[40,44]

For the viewpoint of practical applications, full cell performances are essential for a high capacity anode. However, only a few papers reported the full cell properties of Ge-based anodes.[13,23,45] Herein, Olivine-type $LiFePO_4$ with a perfect reversible Li storage behavior was employed as cathode to be coupled with our Ge microcubes in full cells. Figure 5a presents the voltage profiles of the Ge microcubes/$LiFePO_4$ full cell for the first 10 cycles at 0.1 C. The initial Coulombic efficiency in the full cell is about 80%, which is lower than that in the half cell due to some irreversible lithium loss in the real battery system. The flat charge plateau around 3.1 V for the first cycle is in good accordance with the first lithiation behavior of Ge microcubes shown in Figure 3a. In the subsequent cycles, the shapes of the curves keep constant, indicative of a good reversibility of the full cell system. It is confirmed that, after 100 cycles at 0.5 C, the Ge-based anode still kept a reversible capacity of 1123 mAh g^{-1}, as shown in Figure 4b. Benefited from the unique structure and highly reversible lithium storage behavior, the specific capacity of Ge microcubes at 0.1, 0.5, 1, and 2 C is 1150, 1109, 981, and 782 mAh g^{-1}, respectively, at a fixed lithiation rate of 0.2 C, as displayed in Figure 5c. Additionally, we assembled an LED array which was powered by our Ge-based full cells as shown in Figure S9 (Supporting Information). The two letters were occupied by red and yellow LED bulbs, respectively. It is worth noting that red and yellow LEDs (turn-on voltage 1.9−2.3 V) were employed as light source because the voltage plateau of the cell is around 2.7 V. It is seen clearly form Figure 5d that the full cells could light up the whole LED array. All the bulbs exhibiting favorable brightness confirmed that the Ge microcubes could be applied in practical devices instead of the graphite anode.

DOI: 10.1021/acs.chemmater.5b00218
Chem. Mater. 2015, 27, 2189−2194

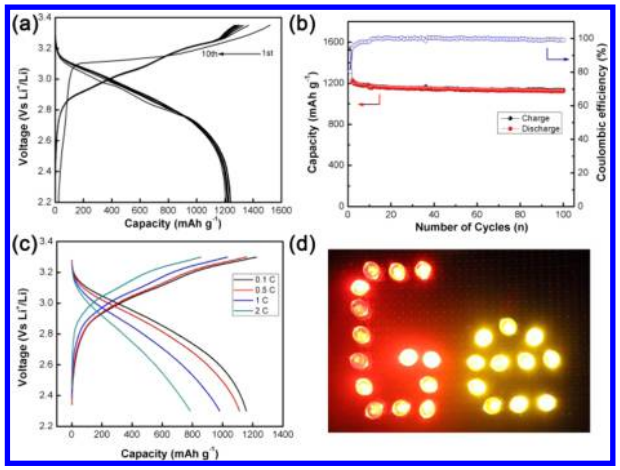

Figure 5. Electrochemical performances of the Ge microcubes/$LiFePO_4$ full cells. The specific capacities are calculated based on the mass of anode. (a) Voltage profiles of the cell cycled for the first 10 cycles between 2.3 and 3.3 V at a rate of 0.1 C. (b) Cycling performance of the full cell at 0.5 C. (c) Rate capability of cell from 0.1 to 2 C. The lithiation rate was kept constant at 0.2 C. (d) Digital photograph of LED array powered by Ge microcubes/$LiFePO_4$ full cells. Because of the difference between the turn-on voltages of the red and yellow LED, the two letters were powered by two individual cells, respectively.

CONCLUSIONS

In summary, we successfully synthesized Ge microcubes composed of nano-building blocks which exhibited a superior initial Coulombic efficiency of 91.8% at the rate of 0.1 C. The good crystallinity and absence of a native oxide layer of the Ge microcubes, as well as free of electrochemical inert additive in the monolithic electrode, were considered to be responsible for this remarkable value by minimizing the irreversible lithium consumption. Stable cycle performances were achieved because of the well-maintained electrode structure integrity before and after cycling. We stress that the micro/nano hierarchical structures of the monolithic electrode combined with the well-formed Li_2CO_3-predominated SEI layers were responsible for the excellent cycling stability and rate performance, although the detailed mechanisms still need further investigation. Convincing full cell properties indicate that the Ge microcubes could be a promising anode for high-performance LIBs for a wide range of applications.

ASSOCIATED CONTENT

Supporting Information

XRD patterns and SEM images of GeO_2 mirocubes, XPS pattern of Ge microcubes, morphology evolution images of Ge nanoparticles during lithium insertion, rate capabilities of the Ge microcubes anode, XPS spectra of the fully lithiated Ge microcubes anode, Nyquist plots of the Li/Ge half cell at different lithiated voltages for the first cycle when discharged at the current density of 10 C, and digital photograph of LED array powered by Ge microcubes/$LiFePO_4$ full cells. This material is available free of charge via the Internet at http://pubs.acs.org.

AUTHOR INFORMATION

Corresponding Authors

*E-mail: cuigl@qibebt.ac.cn (G.C.).
*E-mail: l.gu@iphy.ac.cn (L.G.).

Notes

The authors declare no competing financial interest.

ACKNOWLEDGMENTS

The authors thank the Qingdao Key Lab of Solar Energy Utilization and Energy Storage Technology, the China Postdoctoral Science Foundation (2014M561976), the National Program on Key Basic Research Project of China (973 Program) (No. MOST2011CB935700), the NSFC program (21271180), and the Key Technology Research Projects of Qingdao (No. 13-4-1-10-gx) for financial support.

REFERENCES

(1) Bogart, T. D.; Chockla, A. M.; Korgel, B. A. *Curr. Opin. Chem. Eng.* **2013**, *2*, 286−293.
(2) Chou, C. Y.; Kim, H.; Hwang, G. S. *J. Phys. Chem. C* **2011**, *115*, 20018−20026.
(3) Ren, J. G.; Wu, Q. H.; Tang, H.; Hong, G.; Zhang, W. J.; Lee, S. T. *J. Mater. Chem. A* **2013**, *1*, 1821−1826.
(4) Seng, K. H.; Park, M.-H.; Guo, Z. P.; Liu, H. K.; Cho, J. *Angew. Chem., Int. Ed.* **2012**, *51*, 5657−5661.
(5) Graetz, J.; Ahn, C. C.; Yazami, R.; Fultz, B. *J. Electrochem. Soc.* **2004**, *151*, A698−A702.
(6) Weker, J. N.; Liu, N.; Misra, S.; Andrews, J. C.; Cui, Y.; Toney, M. F. *Energy Environ. Sci.* **2014**, *7*, 2771−2777.
(7) Xue, D. J.; Xin, S.; Yan, Y.; Jiang, K. C.; Yin, Y. X.; Guo, Y. G.; Wan, L. J. *J. Am. Chem. Soc.* **2012**, *134*, 2512−2515.
(8) Kennedy, T.; Mullane, E.; Geaney, H.; Osiak, M.; O'Dwyer, C.; Ryan, K. M. *Nano Lett.* **2014**, *14*, 716−723.
(9) Yuan, F. W.; Yang, H. J.; Tuan, H.-Y. *ACS Nano* **2012**, *6*, 9932−9942.
(10) Chan, C. K.; Zhang, X. F.; Cui, Y. *Nano Lett.* **2007**, *8*, 307−309.
(11) Liu, J.; Song, K.; Zhu, C.; Chen, C. C.; van Aken, P. A.; Maier, J.; Yu, Y. *ACS Nano* **2014**, *8*, 7051−7059.
(12) Chockla, A. M.; Klavetter, K. C.; Mullins, C. B.; Korgel, B. A. *ACS Appl. Mater. Interfaces* **2012**, *4*, 4658−4664.
(13) Park, M. H.; Cho, Y.; Kim, K.; Kim, J.; Liu, M.; Cho, J. *Angew. Chem., Int. Ed.* **2011**, *50*, 9647−9650.
(14) Song, T.; Cheng, H.; Choi, H.; Lee, J.-H.; Han, H.; Lee, D. H.; Yoo, D. S.; Kwon, M. S.; Choi, J. M.; Doo, S. G.; Chang, H.; Xiao, J.; Huang, Y.; Park, W. I.; Chung, Y. C.; Kim, H.; Rogers, J. A.; Paik, U. *ACS Nano* **2011**, *6*, 303−309.
(15) Lu, X.; Korgel, B. A. *Chem.—Eur. J.* **2014**, *20*, 5874−5879.
(16) Yu, Y.; Yan, C.; Gu, L.; Lang, X.; Tang, K.; Zhang, L.; Hou, Y.; Wang, Z.; Chen, M. W.; Schmidt, O. G.; Maier, J. *Adv. Energy Mater.* **2013**, *3*, 281−285.
(17) Guo, Y. G.; Hu, Y. S.; Sigle, W.; Maier, J. *Adv. Mater.* **2007**, *19*, 2087−2091.
(18) Tao, F. F.; Guan, M. Y.; Zhou, Y. M.; Zhang, L.; Xu, Z.; Chen, J. *Cryst. Growth Des.* **2008**, *8*, 2157−2162.
(19) Zhang, H. L.; Zhang, Y.; Zhang, X. G.; Li, F.; Liu, C.; Tan, J.; Cheng, H. M. *Carbon* **2006**, *44*, 2778−2784.
(20) He, Y.; Yu, X.; Wang, Y.; Li, H.; Huang, X. *Adv. Mater.* **2011**, *23*, 4938−4941.
(21) Yang, L. C.; Gao, Q. S.; Li, L.; Tang, Y.; Wu, Y. P. *Electrochem. Commun.* **2010**, *12*, 418−421.
(22) Wachtler, M.; Winter, M.; Besenhard, J. O. *J. Power Sources* **2002**, *105*, 151−160.
(23) Li, X.; Yang, Z.; Fu, Y.; Qiao, L.; Li, D.; Yue, H.; He, D. *ACS Nano* **2015**, *9*, 1858−1867.
(24) Zhang, C.; Pang, S.; Kong, Q.; Liu, Z.; Hu, H.; Jiang, W.; Han, P.; Wang, D.; Cui, G. *RSC Adv.* **2013**, *3*, 1336−1340.
(25) Gu, M.; Wang, Z.; Connell, J. G.; Perea, D. E.; Lauhon, L. J.; Gao, F.; Wang, C. *ACS Nano* **2013**, *7*, 6303−6309.
(26) Liang, W.; Yang, H.; Fan, F.; Liu, Y.; Liu, X. H.; Huang, J. Y.; Zhu, T.; Zhang, S. *ACS Nano* **2013**, *7*, 3427−3433.
(27) Cui, G. L.; Gu, L.; Zhi, L. J.; Kaskhedikar, N.; van Aken, P. A.; Müllen, K.; Maier, J. *Adv. Mater.* **2008**, *20*, 3079−3083.

DOI: 10.1021/acs.chemmater.5b00218
Chem. Mater. 2015, 27, 2189−2194

(28) Jia, H.; Kloepsch, R.; He, X.; Badillo, J. P.; Gao, P.; Fromm, O.; Placke, T.; Winter, M. *Chem. Mater.* **2014**, *26*, 5683−5688.
(29) Ke, F. S.; Mishra, K.; Jamison, L.; Peng, X. X.; Ma, S. G.; Huang, L.; Sun, S. G.; Zhou, X. D. *Chem. Commun.* **2014**, *50*, 3713−3715.
(30) Wu, H. B.; Chen, J. S.; Hng, H. H.; Wen Lou, X. *Nanoscale* **2012**, *4*, 2526−2542.
(31) Zhou, L.; Zhao, D. Y.; Lou, X. W. *Adv. Mater.* **2012**, *24*, 745−748.
(32) Wang, L. Z.; Tang, F. Q.; Ozawa, K.; Chen, Z. G.; Mukherj, A.; Zhu, Y. C.; Zou, J.; Cheng, H. M.; Lu, G. Q. *Angew. Chem., Int. Ed.* **2009**, *48*, 7048−7051.
(33) He, Y.; Piper, D. M.; Gu, M.; Travis, J. J.; George, S. M.; Lee, S.-H.; Genc, A.; Pullan, L.; Liu, J.; Mao, S. X.; Zhang, J.-G.; Ban, C.; Wang, C. *ACS Nano* **2014**, *8*, 11816−11823.
(34) Baggetto, L.; Notten, P. H. L. *J. Electrochem. Soc.* **2009**, *156*, A169−A175.
(35) Seo, M. H.; Park, M.; Lee, K. T.; Kim, K.; Kim, J.; Cho, J. *Energy Environ. Sci.* **2011**, *4*, 425−428.
(36) Chan, C. K.; Ruffo, R.; Hong, S. S.; Cui, Y. *J. Power Sources* **2009**, *189*, 1132−1140.
(37) Li, J.; Dudney, N. J.; Xiao, X.; Cheng, Y. T.; Liang, C.; Verbrugge, M. W. *Adv. Energy Mater.* **2014**, DOI: 10.1002/aenm.201401627.
(38) Choi, Y. K.; Chung, K. I.; Kim, W. S.; Sung, Y. E.; Park, S. M. *J. Power Sources* **2002**, *104*, 132−139.
(39) Xiao, L.; Wu, D.; Han, S.; Huang, Y.; Li, S.; He, M.; Zhang, F.; Feng, X. *ACS Appl. Mater. Interfaces* **2013**, *5*, 3764−3769.
(40) Kohandehghan, A.; Cui, K.; Kupsta, M.; Ding, J.; Memarzadeh Lotfabad, E.; Kalisvaart, W. P.; Mitlin, D. *Nano Lett.* **2014**, *14*, 5873−5882.
(41) Nie, M.; Abraham, D. P.; Seo, D. M.; Chen, Y.; Bose, A.; Lucht, B. L. *J. Phys. Chem. C* **2013**, *117*, 25381−25389.
(42) Zhang, S. S.; Xu, K.; Jow, T. R. *Electrochim. Acta* **2006**, *51*, 1636−1640.
(43) Yan, C. L.; Xi, W.; Si, W. P.; Deng, J. W.; Schmidt, O. G. *Adv. Mater.* **2013**, *25*, 539−544.
(44) Chou, C. Y.; Hwang, G. S. *J. Power Sources* **2014**, *263*, 252−258.
(45) Yuan, F. W.; Tuan, H. Y. *Chem. Mater.* **2014**, *26*, 2172−2179.

DOI: 10.1021/acs.chemmater.5b00218
Chem. Mater. 2015, 27, 2189−2194